DOI: 10.1021/ma900384b

Macromolecules
ARTICLE

# Thermodynamic Characterization of Polymorphs in Bulk-Crystallized Syndiotactic Polystyrene via Small/Wide-Angle X-ray Scattering and Differential Scanning Calorimetry

**C. H. Su,[†,‡] U. Jeng,*[,†] S. H. Chen,[§] C.-Y. Cheng,[†] J.-J. Lee,[†] Y.-H. Lai,[†,∥] W. C. Su,[⊥] J. C. Tsai,[#] and A. C. Su*[,‡,&]**

[†]*National Synchrotron Radiation Research Center, Science-based Industrial Park, Hsinchu 300, Taiwan,* [‡]*Institute of Materials Science and Engineering, National Sun Yat-sen University, Kaohsiung 824, Taiwan,* [§]*Department of Materials Science and Engineering, National Dong Hwa University, Hualien 974, Taiwan,* [∥]*Department of Chemistry, Tunghai University, Taichung, 407, Taiwan,* [⊥]*Department of Civil Engineering, National Chiao Tung University, Hsinchu 300, Taiwan,* [#]*Department of Chemical Engineering, National Chung Cheng University, Chiayi 621, Taiwan, and* [&]*Department of Chemical Engineering, National Tsing Hua University, Hsinchu 300, Taiwan*

*Received February 19, 2009; Revised Manuscript Received April 11, 2009*

ABSTRACT: By means of in situ small/wide-angle X-ray scattering (SAXS/WAXS) and differential scanning calorimetry (DSC), we examined evolutions of lamellar crystal thickness for α and $\beta$ crystals, respectively, in bulk-crystallized syndiotactic polystyrene (sPS) during the partial melting−reorganization process upon progressive heating up to 290 °C. For the SAXS data analysis, the Kratky−Porod approximation proves to be particularly helpful in extracting the crystal thickness when approaching final melting where crystalline lamellae (near equilibration with the melt) exist in low concentrations as dispersed entities instead of in arrays. On the basis of the crystal thicknesses at elevated temperatures under solid−melt equilibration, we constructed melting lines of the two separate forms in the Gibbs−Thomson phase plane. The extrapolated (to infinite lamellar thickness) equilibrium melting temperature $T_{m,\alpha}^* \approx 294$ °C of the α form is moderately lower than $T_{m,\beta}^* \approx 306$ °C of the $\beta$ form. The two melting lines intercept at a crossover temperature $T_Q \approx 284$ °C and crystal thickness $l_Q \approx 9.6$ nm, where the relative thermal stability of the two phases inverses. For crystals thicker than $l_Q$ (practically hard to reach for bulk crystallization under ambient pressure), the $\beta$ form is the stable phase; for crystals thinner than $l_Q$ (the commonly accessible case), the α form is *circumstantially* more stable. With crystallinity-corrected values of the heat of fusion $\Delta H_{f,\alpha} \approx 82$ MJ m$^{-3}$ and $\Delta H_{f,\beta} \approx 146$ MJ m$^{-3}$ obtained from a combination of DSC and WAXS results, we determined from the slope ($= 2\sigma_e/\Delta H_f$) of the melting line that basal surface energy $\sigma_{e,\alpha} \approx 8.2$ mJ m$^{-2}$ and $\sigma_{e,\beta} \approx 26.8$ mJ m$^{-2}$, which are considerably lower than those expected for tight folds, indicative of nonadjacently re-entered or loosely looped folds. The combination of lower $T_m^*$, $\Delta H_f$, $\Delta S_f$, and $\sigma_e$ values renders the α phase highly competitive in the rate of nucleation at low temperatures but much less so at high temperatures as compared to the $\beta$ phase. The higher $\sigma_{e,\beta}$ value is also consistent with the observation that the $\beta$ phase is more responsive to externally added heterogeneous nucleation agents.

## Introduction

Syndiotactic polystyrene (sPS) has been extensively studied since the first successful synthesis[1] around 1985. For bulk-crystallized sPS in the absence of a solvent, there are two main polymorphs coined as α and $\beta$ phases; both consist of *all-trans* chains.[2] The α phase is composed of *frustrated* arrangement[3] with azimuthal settings of hexagonal columns ("triplets", each comprising three chains), hence trigonal (space group $P3$) in structure, forming a nine-chain unit cell of dimensions $a = b = 2.626$ nm, $c = 0.504$ nm, and density $\rho = 1.033$ g cm$^{-3}$ at room temperature. The $\beta$ phase is more boardlike, orthorhombic (space group $P2_12_12_1$) in structure, and comprises four chains in a unit cell of $a = 0.881$ nm, $b = 2.882$ nm, and $c = 0.506$ nm with $\rho = 1.067$ g cm$^{-3}$. For the sake of simplicity, we have neglected subcategories (α′, α″, $\beta'$, and $\beta''$) in which the presence of packing disorder is further considered.[2,4]

In contrast to structural characteristics, understanding in thermodynamic properties of the two phases, however, remains unsatisfactory. In a number of studies[5−11] devoted to determining the equilibrium melting temperatures ($T_m^*$) for the α and $\beta$ phases of sPS, results are widely scattered due presumably to the limitations of the adopted methodologies and/or phase impurity. In the analysis of differential scanning calorimetric (DSC) measurements, the often adopted Hoffman−Weeks analysis (HW)[12] and its nonlinear version proposed by Marand et al. (nonlinear HW)[13,14] are both based on Lauritzen−Hoffman theory, albeit with further simplifying assumptions that are less than adequately justified.[15] As shown in Table 1, reported estimates for $T_m^*$ of the α phase ranged from 273 to 298 °C whereas those of the $\beta$ phase ranged from 279 to 320 °C. In one typical study, Ho et al.[5] analyzed their DSC results with both linear and nonlinear HW methods for the $T_m^*$ values: HW-determined $T_m^*$ values were substantially lower (by 23−29 °C) than those extracted with the nonlinear HW method. We note that Alamo et al.[16] have shown conclusively that the lamellar thickening coefficient exhibits significant temperature dependence, in disfavor of the linear HW analysis.

*To whom correspondence should be addressed.

 Published on Web 05/21/2009 

**Table 1. Previously Reported Values (in °C) of Equilibrium Melting Temperatures for sPS[a]**

| | phase unidentified | | α phase | | | β phase | | |
|---|---|---|---|---|---|---|---|---|
| reference | HW | GT | HW | NHW | GT | HW | NHW | GT |
| 2 | | | 282 | | | 289 | | |
| 5 | | | 273 | 298 | | 279 | 307 | |
| 6 | | | 289 | | | 283 | | |
| 7 | | | 281 | 294 | | 291 | 320 | |
| 8 | | | | | 281 | | | 293 |
| 9 | | | | | | 286 | | |
| 10 | 275 | | | | | | | |
| 11 | | 279 | | | | | | |

[a] HW: linear Hoffman−Weeks method; NHW: nonlinear Hoffman−Weeks extrapolation; GT: Gibbs−Thomson approach.

By use of the Gibbs−Thomson (GT) relation, Wang et al.[7,8] extrapolated the respective $T_m$* values of 281 and 293 °C for the α and β phases of sPS from melting temperatures $T_m$ and lamellar crystalline thickness $l_c$ determined via DSC and SAXS, respectively. However, the $l_c$ values were extracted from SAXS profiles obtained either at room temperature (for the β phase) or at 180 °C (for the α phase), quite distant from the corresponding $T_m$ determined via DSC as the final melting temperature and hence are inappropriate to represent for the thickened lamellae at $T_m$. There are also reported $T_m$* values for sPS using samples of unspecified phase or coexisting phases.[10,11] Although more recent high-temperature wide-angle X-ray scattering results have raised the lower bound somewhat to 286 °C for the α phase and 280 °C for the β phase,[17] the range of uncertainty in $T_m$* is still disturbingly large for each phase.

In addition, the popularly recognized estimate for the heat of fusion $\Delta H_f = 8.6$ kJ mol$^{-1}$ at 100% crystallinity was determined some 18 years ago[18] *without* phase specification (as the polymorphic nature of sPS was yet unknown) via fitting of experimentally determined melting temperature ($T_m$) *in the presence of diluents*, with the Flory's solution-based theory. With simultaneously determined bulk $T_m$ of 269 °C, the corresponding entropy of fusion was given as $\Delta S_m = 16$ J K$^{-1}$ mol$^{-1}$.[18] A separate estimate was $\Delta H_f = 5.5$ kJ mol$^{-1}$ slightly later.[19] These $\Delta H_f$ values were often adopted in subsequent studies[7,8,20] by assuming its applicability to *both* the α and β phases, which is certainly questionable in view of the significant difference (>3%) in density. In fact, the density of the α phase is even lower than that of the amorphous phase ($\rho \approx 1.04$ g mL$^{-1}$) at room temperature, leading to the re-entrant behavior in the pressure−temperature phase diagram.[21]

In spite of uncertainties in the exact values of $T_m$*, it is generally believed[2] that, although α crystals are often higher in $T_m$, their extrapolated $T_m$* value (via either the Hoffman−Weeks plot[12] or the more sophisticated version of Marand et al.[13,14]) is lower than that of the β phase; i.e., the β phase is thermodynamically the stable phase for thick crystals at elevated temperatures. Considering *circumstantial* metastability[22] with effects from $l_c$ incorporated, Ho et al.[5,23] constructed a relative phase stability diagram for the two phases in the $T_m - l_c^{-1}$ plane, where the crossover point ($T_Q$, $l_Q^{-1}$) of the two schematic Gibbs−Thomson (GT) melting lines signifies a stability inversion—based on which the observed α-to-β transformation (considered *not* as a traditional solid−solid transformation but rather through surface reorganization in terms of a floating-chain picture) was qualitatively explained. This conditional α-to-β transformation, however, was *not* confirmed in subsequent wide-angle X-ray scattering (WAXS) investigations[17,24] in the temperature range of 240−270 °C or even up to 286 °C. Apparently, reliable GT lines for the two phases and hence quantitative information on the crossover point ($T_Q$, $l_Q^{-1}$) are needed in clarifying these results on the phase transformation.

The determination of GT lines for the α and β forms of sPS, however, is not as trivial as it might first appear. There were published attempts[8,25] to give GT lines via a combination of routine DSC analysis for $T_m$ and a low (typically ambient) temperature small-angle X-ray scattering (SAXS) for $l_c$, but the few data points were highly scattered and hence gave limited confidence after long extrapolation. As we have briefly commented, previous attempts suffered ambiguities in analyzing the polymer crystals with either a broad DSC endotherm or multiple endotherms. While the simplified SAXS analysis gave only the average lamellar thickness at a low temperature, the DSC-determined $T_m$ corresponded to either the melting of thin crystals (if initial melting was used for determination of $T_m$) or to thick lamellae (if the final melting maximum was taken as $T_m$). In this type of approach, there are also kinetic effects from finite heating rates[5] that need to be corrected (but often omitted,[7,8,25] as uncertainties could sometimes further grow with this procedure). To avoid such complications, Al-Hussein and Strobl[15,26] recently measured average lamellar crystal thickness for several semicrystalline polymers via SAXS with rising temperature at small increments. In this improved approach with gradual temperature rise, thin crystals either melt away or thicken into crystals of a narrower distribution that approach solid−melt equilibration at high temperatures; therefore, with crystals of a series of initial crystal thicknesses, the high-temperature tails of the (generally curved) $T - l_c^{-1}$ trajectories converge into a straight envelope of reliable Gibbs−Thomson line. A practical problem might arise with typical in-house SAXS instruments though: the prolonged high-temperature history due to long data acquisition periods could lead to polymer degradation; this concern, however, is easily avoidable in the case of high brilliance synchrotron-radiation X-ray sources.

Here we report results of our recent efforts in thermodynamic characterization of bulk-crystallized sPS by adopting the incremental temperature scheme of Strobl[15,26] but using synchrotron-based, simultaneous SAXS/WAXS/DSC instead, which avoids interferences from thermal degradation and, more importantly, eliminates fundamental errors in correlating the average lamellar thickness at a low temperature to DSC-determined $T_m$ (with complications from effects of partial melting or reorganization processes during heating) in the earlier studies. We therefore expect more accurate construction of GT lines in the $T_m - l_c^{-1}$ plane for the α and β phases. In addition, we have used the Kratky−Porod (KP) approximation[27] in our SAXS data analysis to determine the crystal thickness at temperatures closer to solid−melt equilibration where stacking order of crystalline lamellae deteriorates, hampering the reconstruction of the layer structure (hence the determination of crystal thickness) from one-dimensional (1-D) correlation function.[27,28] Furthermore, on the basis of DSC and WAXS results, we have quantitatively determined the crystallinity-corrected heat of fusion ($\Delta H_f$) for the two phases, which in turn gives value of the fold surface energy ($\sigma_e$) from the slope of the corresponding GT line. With these values of thermodynamic parameters, bulk crystallization behavior of sPS is discussed in definite terms.

## Experimental Section

**Materials.** The syndiotactic polystyrene sample with weight-average molecular mass $M_w = 140$ kDa, polydispersity of 2.4, and high stereoregularity (>98% in [*rr*] triad content as determined from $^{13}$C nuclear magnetic resonance spectroscopy)[29] was obtained from the Grand Pacific Petrochemical and was purified via precipitation of hot xylene solution into a large excess of methanol. The sample was then melted and consolidated under a protective nitrogen atmosphere at 300 °C in a Linkman THMS-600 temperature stage that was calibrated to within ±0.5 °C using benzoic acid, 2-chloroanthaquinone, and $KNO_3$.

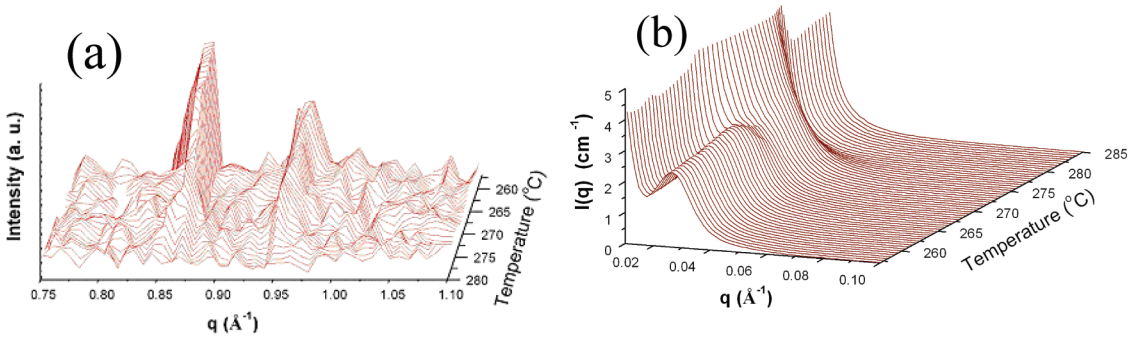


**Figure 1.** Representative (a) WAXS and (b) SAXS profiles obtained during heating of specimen $\beta$-254 (melt-crystallized at 254 °C for 20 min) at 1.5 °C min$^{-1}$ from 254 to 285 °C. Note the characteristic (040) and (130) reflections of the $\beta$ phase at $q = 0.85$ and 0.95 Å$^{-1}$, respectively.

Specimens containing purely $\beta$ crystals were prepared in a Mettler Toledo FP84 differential scanning calorimeter (DSC) cell. After heated to 300 °C for 1 min to erase all previous thermal history, specimens were melt crystallized under the protective nitrogen atmosphere at a temperature $T_{mc}$ chosen between 244 and 258 °C for 10−60 min. Specimens containing predominantly α crystals were prepared in a more elaborate manner. After heating to 300 °C for 1 min, specimens were quenched into ice water. The glassy specimens were then individually cold-crystallized at a selected temperature $T_{cc}$ between 220 and 260 °C, for a period up to 90 min before quenched into liquid nitrogen. There existed some residual $\beta$ phase (≤13% of all crystals) in the α-dominated specimens as determined by means of wide-angle X-ray scattering (WAXS);[30] effects from these residual $\beta$ crystals were corrected (by subtracting their contributions to the melting endotherm of the α-dominated specimen) to retrieve the thermodynamic parameters of the pure α phase.

**Simultaneous SAXS/WAXS/DSC.** Simultaneous small-angle X-ray scattering (SAXS), WAXS, and DSC measurements were performed at the wiggler beamline BL17B3 of the National Synchrotron Radiation Research Center (NSRRC).[31] Specimens ca. 1.0 mm in thickness and 6 mm in diameter were respectively sealed in Al pans with Kapton windows ca. 2 mm in diameter for the X-ray beam. The Al sample cell was then placed in the cell holder of the Mettler Toledo FP84 instrument modified for simultaneous SAXS/WAXS/DSC measurements, as detailed elsewhere.[32] With an 8 keV (wavelength $\lambda = 1.55$ Å) beam, SAXS and WAXS data were respectively collected using 2-D (200 × 200 mm$^2$) and 1-D (200 mm) gas-type linear proportional counters in a master-slave mode during heating from 220 to 290 at 1.5 °C/min. Constrained by geometry of the SAXS/WAXS/DSC setup, the corresponding sample-to-detector distances used for the SAXS and WAXS detectors were 2730 and 750 mm, respectively. This setup resulted in a limited WAXS $q$-range of 0.8−1.5 Å$^{-1}$ but a favorable SAXS $q$-range of 0.006−0.25 Å$^{-1}$. The scattering wavevector $q \equiv 4\pi\lambda^{-1} \sin\theta$ (with $2\theta$ the scattering angle) was calibrated under the same sPS sample environment using silver behenate for SAXS and polyethylene/tripalmitate/poly(ε-caprolactone) for WAXS. Fluorescence spectra from an iron sheet were used to calibrate the pixel sensitivity of the SAXS and WAXS detectors; all SAXS and WAXS data were corrected for sample transmission, background scattering, and detector noise. The SAXS data were placed in the absolute intensity scale by use of a precalibrated high-density polyethylene standard.

To better determine the crystallinity of the samples with WAXS spectra of a wider $q$ range, a separate set of simultaneous WAXS/DSC experiments were performed at the BL17A powder X-ray diffraction beamline of NSRRC with 9.34 keV (1.327 Å) X-rays and a MAR345 2-D detector of 380 × 250 mm$^2$ imaging area.

**Data Analysis.** Lamellar crystal thickness ($l_c$) of the semicrystalline sPS was extracted with the 1-D correlation function $\gamma_1(z)$ Fourier-transformed from the corresponding 1-D SAXS intensity profile $I(q)$ measured, using the procedures detailed in our previous reports.[30,33] Before the Fourier transformation, SAXS data in the high-$q$ region were corrected for thermal fluctuation effects and extrapolated using the Porod−Ruland model, whereas data in the low-$q$ region were extrapolated with the Debye−Bueche relation. Close to crystal melting, where the lamellar structure significantly deteriorates, $l_c$ could not be extracted reliably from $\gamma_1(z)$, as there was no clearly defined crystal long period. In such case, crystal thickness of the disordered crystal blocks was directly extracted from the form factor scattering using the Kratky−Porod (KP) approximation[27] that $I(q) \propto q^{-2} \exp(-q^2 l_c^2/12)$ for slablike scattering objects.[34,35] The crystal thickness $l_c$ can be extracted from the slope ($= l_c^2/12$) of the corresponding KP plot of $\ln[I(q)q^2]$ vs $q^2$. The KP approximation is valid within the range of $\pi/R < q < 2\pi/l_c$, where $2R$ ($\gg l_c$) is the lateral dimension of the slablike entities.

The relative crystallinity $X_{c,WAXS}$ was obtained from the integrated intensity over the observed Bragg reflections normalized by that over the whole WAXS profile. The sample heat flow from DSC was calibrated with In/Pb/Sn and corrected for the sample mass for the heat of fusion ($\Delta H_f$), which was further normalized by $X_{c,WAXS}$ for the specific $\Delta H_f$ of the corresponding crystalline phase. For the case of α phase, the heat flow and $X_{c,WAXS}$ measured from the α-dominated samples were corrected for the contribution of the residual $\beta$ crystals.

## Results and Discussion

**Melting Line of the $\beta$ Phase.** Given in Figure 1 are representative WAXS/SAXS profiles of a $\beta$-dominated specimen (melt crystallized at $T_{mc} = 254$ °C and hence denoted as $\beta$-254) obtained during heating from 254 to 284 °C. Without discernible contributions from the α form, the WAXS profiles showed predominating presence of the characteristic $(040)_\beta$ and $(130)_\beta$ reflections of the $\beta$ phase at $q = 0.85$ and 0.95 Å$^{-1}$. Intensities of the two reflections decreased clearly with increasing temperature above 265 °C and faded into the background near 278 °C. Concurrently, the DSC trace (Figure 2a) gave two melting endotherms located respectively at $T_{m1,\beta} = 268$ °C and $T_{m2,\beta} = 277$ °C. The first endotherm, usually located 10−15 °C above the corresponding $T_{mc}$, is attributed to the melting of thinner crystallites; the second endotherm corresponds to the melting of pre-existing thick crystallites or those thickened during heating. Consistent with this interpretation, changes in the corresponding SAXS profiles (Figure 1b and more clearly presented in Figure 2b) demonstrate a significant low-$q$ shifting in the lamellar peak position (initially located at $q = 0.026$ Å$^{-1}$) after $T_{m1}$. Once heated above $T_{m2,\beta}$, the lamellar peak (i.e., the layer structure) diminishes quickly,

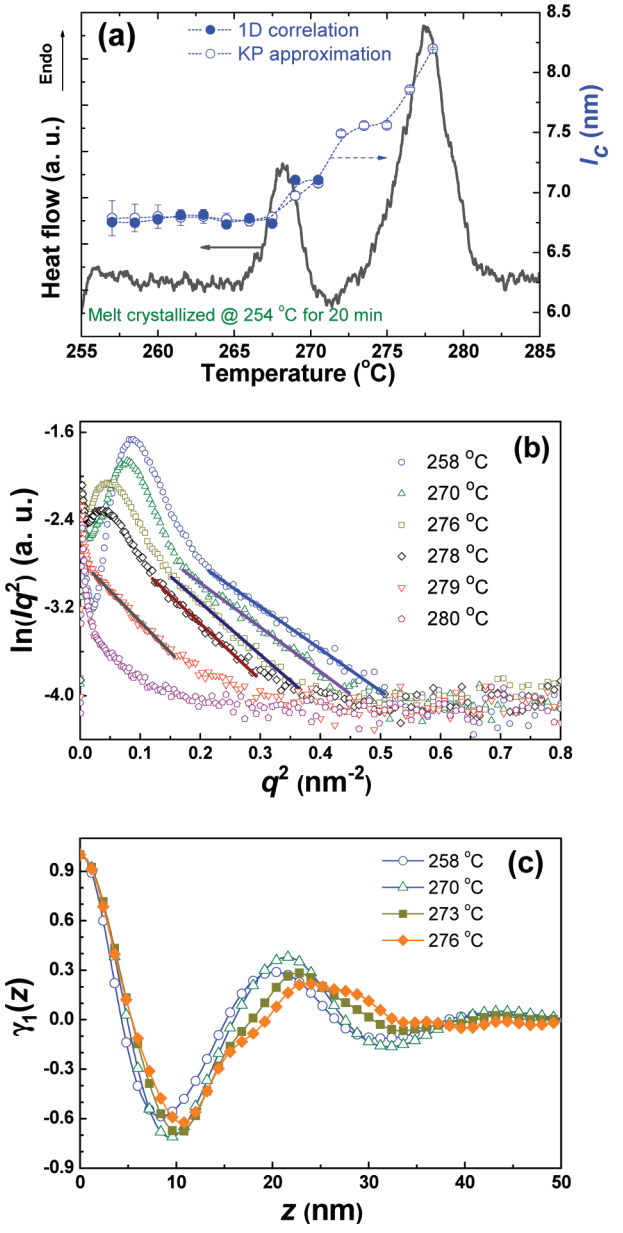


**Figure 2.** (a) DSC heating trace (solid curve) for the $\beta$-dominated specimen $\beta$-254, along with values of crystal thickness (scale given at right) extracted from the 1-D correlation function and those from the Kratky−Porod (KP) approximation. (b) SAXS data in the KP presentation are fitted with the KP approximation (solid lines). (c) Representative 1-D correlation functions Fourier transformed from the SAXS profiles of $\beta$-254 during heating.

due presumably to the melting of the final, thick crystals. All eight sets of SAXS/WAXS/DSC data for the $\beta$-dominated specimens melt crystallized at $T_{mc}$ = 244−258 °C (in 2 °C intervals) behave similarly.

Given in Figure 2c are 1-D correlation functions $\gamma_1(z)$ obtained from the SAXS profiles in Figure 1b, from which temperature-dependent crystal thickness between 6.5 and 7.0 nm can be determined (see Figure 2a) below $T_{m2,\beta}$. Near $T_{m2,\beta}$, however, the $\gamma_1$ function starts to distort from the typical shape of a well-behaved lamellar structure (e.g., the case of 258 °C), and the situation deteriorates with the quickly diminished lamellar peak (Figures 1b and 2b) in the SAXS profile upon further increase in temperature. For such case, the crystal thickness is more appropriately extracted with the Kratky−Porod (KP) approximation

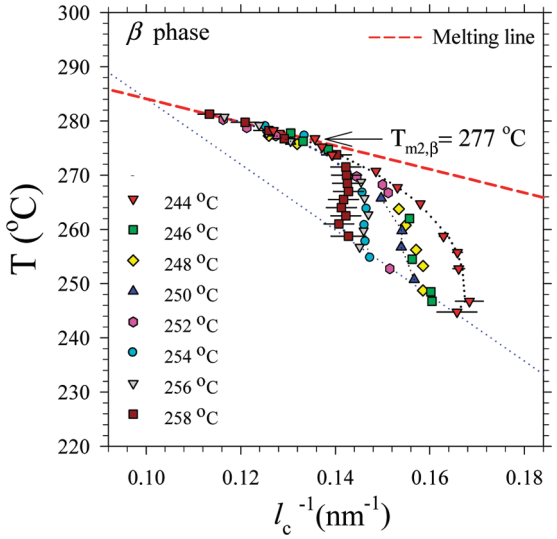


**Figure 3.** Evolution of crystal thickness ($l_c$) with increasing temperature upon heating at 1.5 °C min$^{-1}$ for the $\beta$-dominated sPS specimens isothermal crystallized at temperatures between 244 and 258 °C. The melting line is fitted from final points of the eight trajectories. The dotted line connects the eight initial crystal thicknesses.

(Figure 2b). As shown in Figure 2a, crystal thickness values determined from the conventional $\gamma_1$ and the KP approaches agree well at lower temperatures when both methods are applicable. At higher temperatures where melting of thinner interstitial crystallites results in disruption of lamellar arrays before final crystal melting (near 280 °C), the KP approach is superior to the 1-D correlation function in determining the few final points of crystal thickness, which are crucial in the determination of the equilibrium melting line: these few final points correspond closely to solid−melt equilibration, as further delineated below. Around 268 °C, $l_c$ shows a steplike sharp increase to 7.5 nm at 272 °C and then remains approximately constant between 272 and 275 °C. Entering the main endotherm at $T$ > 275 °C, the average thickness of the $\beta$ crystals increases further to ca. 8.2 nm before final melting at 277 °C. There is generally no significant thickening prior to the step increases in $l_c$, and each steep increase corresponds to the melting of either the thin lamellae ($T_{m1,\beta}$) or the thinner population among the thick lamellae ($T_{m2,\beta}$). It hence appears that the present case of sPS is closer to the bimodal distribution model of Basset;[36,37] contributions from "continuous melting−reorganization during heating" are insignificant in sPS even at a modest heating rate of 1.5 °C/min.

In Figure 3, the SAXS-deduced reciprocal crystalline lamellar thickness ($l_c^{-1}$) is plotted against the experimental temperature ($T$) for all $\beta$-dominated specimens. At temperatures far below $T_{m2,\beta}$ (≈277 °C), diverse trajectories of the eight specimens in the $T-l_c^{-1}$ plane reflect the fact that these crystalline lamellae are not in equilibrium with the melt: there are increasingly higher populations of crystals with $T_m > T_{mc}$ as $T_{mc}$ is decreased from 258 to 244 °C. The initials of the trajectories (i.e., initial crystal thicknesses), however, fall into a line, as that similarly observed by Strobl with several other semicrystalline polymers.[26] Such behavior associates closely with crystallization kinetics and is out of the scope of current study focusing on thermodynamics characterization. On the other hand, at temperatures higher than $T_{m2,\beta}$, thin crystals have either melted away or thickened to maintain near-equilibration with the melt. Consequently, all the trajectory tails merge into a single envelope, representing the melting line that extrapolates to $T_m^*$ = 306 ± 3 °C

(Figure 3) according to the Gibbs−Thomson relation $T_m = T_m^*(1 - 2\sigma_e/l_c\Delta H_f)$. We note that this $T_m^*$ value for the $\beta$ phase is in better agreement with those (particularly the value of 307 °C obtained by Ho et al.[5] where heating rate effects were careful corrected) derived using Marand's nonlinear extrapolation scheme;[5,7] in contrast, the conventional Hoffman−Weeks linear extrapolation gives significantly lower estimates,[2,5,7] as the assumption of constant lamellar thickening coefficient is clearly inappropriate from the observed evolution of $l_c$ here (Figure 2a).

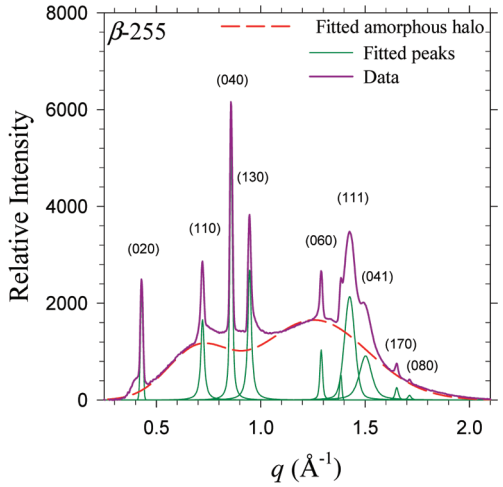


**Figure 4.** Room-temperature WAXS spectrum of the $\beta$-dominated specimen $\beta$-255, with the fitted reflections indexed. Note that the broad amorphous halo is fitted as a linear combination of the two amorphous profiles of the same specimen obtained respectively at 290 °C and at room temperature after liquid nitrogen quenching from 290 °C.

Following the procedures detailed previously for the correction of WAXS-determined crystallinity, we have furthermore extracted an averaged $\Delta H_{f,\beta} = 137 \pm 6$ J g$^{-1}$ = $146 \pm 7$ MJ m$^{-3}$ for the $\beta$ phase from the in situ DSC/WAXS results of $\beta$-250 and $\beta$-255 specimens. Shown in Figure 4 is the full-range room-temperature WAXS profile of $\beta$-255, which corresponds to a relative crystallinity[38] of ca. 27%. With these $T_{m,\beta}^*$ and $\Delta H_{f,\beta}$ values, the fold surface energy of the $\beta$ phase $\sigma_{e,\beta} = 26.8 \pm 1.9$ mJ m$^{-2}$ is derived from the slope of the melting line.

**Melting Line of the α Phase.** Four α-dominated specimens (denoted as α-220, α-230, α-250, and α-260) were prepared by cold crystallization of quenched sPS glass at 220, 230, 250, and 260 °C, respectively. Simultaneously measured SAXS/WAXS/DSC data of these specimens were similarly analyzed as in the case for the $\beta$ phase samples. Shown in Figure 5a−c are representative traces obtained for α-220 upon a heating process from 220 to 290 °C. In Figure 5a, intensities of the characteristic $(300)_\alpha$ and $(220)_\alpha$ reflections of the α phase start to decrease around 255 °C and recede into background near 280 °C. Peak positions of the reflections remain the same during the entire heating process without emergence of $\beta$-related reflections (such as $(040)_\beta$ and $(130)_\beta$ in Figure 1a), showing no signs of α-to-$\beta$ phase transition. The corresponding DSC trace (Figure 5c) displays a hint of initial melting around $T_{m1,\alpha} = 245$ °C and more globally a broad melting endotherm peaked at $T_{m2,\alpha} = 275$ °C. Such a result is attributable to widely distributed crystal thickness in the α phase, presumably a consequence of nuclei formed at widely

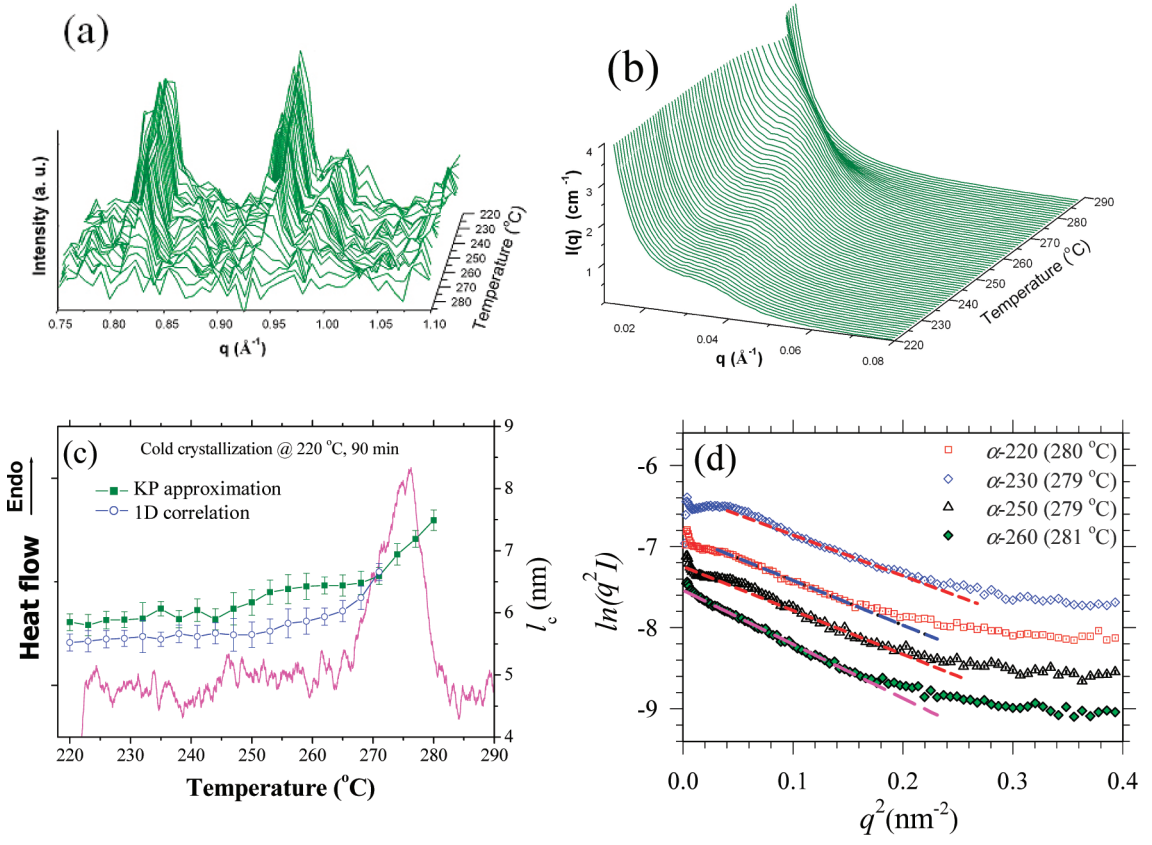


**Figure 5.** (a) Representative WAXS spectra of the α-dominated specimen α-220 during heating process from 220 to 290 at 1.5 °C min$^{-1}$, with the two signature reflections of the α phase, (300) and (220), located at $q = 0.82$ and 0.94 Å$^{-1}$. (b) Corresponding SAXS profiles. (c) DSC trace and the corresponding crystal thicknesses extracted respectively from KP approximation and 1-D correlation function. (d) SAXS profiles of the four α-dominated specimens (isothermally crystallized at temperatures between 220 and 260 °C) at the final melting temperatures (as indicated). Dashed lines correspond to the KP fitting.

**Table 2. Thermodynamics Parameters of the α and β Phases of sPS[a]**

| | $\rho$ (g cm$^{-3}$) | $T_m$* (K) | $\Delta H_f$ (MJ m$^{-3}$) | $\sigma_e$ (mJ m$^{-2}$) | $g$ (kJ mol$^{-1}$) | $\Delta S_f$ (kJ m$^{-3}$ K$^{-1}$) |
|---|---|---|---|---|---|---|
| α | 1.033 | 567 ± 4 | 82 ± 4 | 8.2 ± 1.8 | 6.6 ± 1.4 | 144 ± 7 |
| β | 1.067 | 579 ± 2 | 146 ± 7 | 26.8 ± 1.9 | 20.4 ± 1.4 | 252 ± 12 |

[a] $\rho$ denotes the density, $T_m$* the equilibrium melting temperature, $\Delta H_f$ the heat of fusion, $\sigma_e$ the fold surface energy, $g$ the fold energy, and $\Delta S_f$ the entropy of fusion. Corrections were made to account for the residual β phase in the α-dominated specimens to deduce the parameters for the pure α phase.

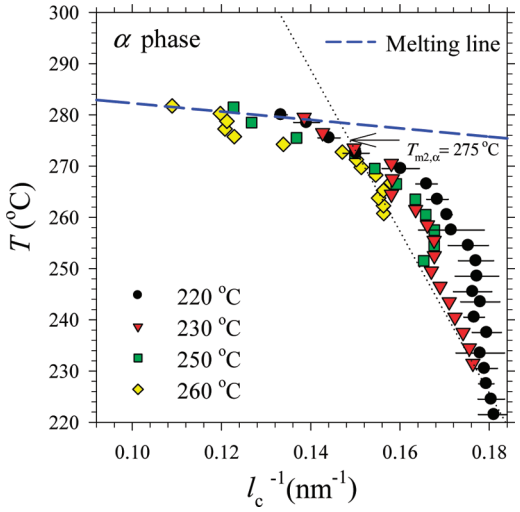


**Figure 6.** Temperature-dependent evolution of reciprocal crystal thickness ($l_c^{-1}$) for the four α-dominated specimens cold crystallized separately at 220, 230, 250, and 260 °C. The GT melting line is determined from the linear envelop formed by the final data points. The dotted line connects the four initial crystal thicknesses.

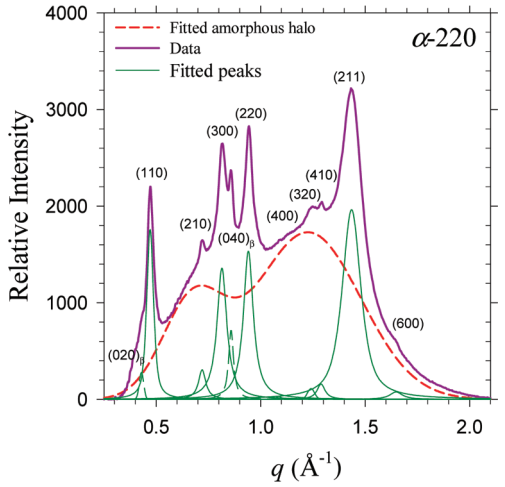


**Figure 7.** Room-temperature WAXS spectrum of the α-dominated specimen α-220 (cold-crystallized at 220 °C), with fitted reflections corresponding to an overall 34% crystallinity respectively contributed by α (29.7%) and β (4.3%) crystals. The fitted amorphous halo is a hybrid of the two different amorphous halos obtained respectively at 290 °C in the melt state and at room temperature as a quenched glass.

different temperatures (and hence of widely different thicknesses upon further thickening/growth) during heating to $T_{cc}$ for isothermal crystallization. Consistent with this interpretation, Figure 5b demonstrates relatively broadened lamellar peaks in the corresponding SAXS profiles, as compared to that of the β phase (Figure 2b). Analogous to the case of β crystals, as temperature reached $T_{m2,\alpha}$ and above, this broad peak shifts quickly toward lower $q$ values before disappearance at ca. 280 °C. We note that the broad lamellar peaks (covering a wider $q$ range) lead to the slightly larger (by ca. 0.5 nm) $l_c$ values with the KP approximation, as compared to that from 1-D correlation function (Figure 5c); with largely diminished lamellar peaks at high temperatures, the final few $l_c$ values are more accurately extracted with the KP approximation (Figure 5d).

In the evolution of the crystal thickness of the α-220 specimen determined from the SAXS data via the KP approximation (Figure 5c), there are no discernible changes in lamellar thickness ($l_c \approx 5.9$ nm) below $T_{m1,\alpha}$; $l_c$ shows a steplike increase to 6.4 nm around 250 °C and then remains approximately constant up to ca. 270 °C. Entering the main endotherm at $T > 270$ °C, the thickness of the α crystals increases steeply to ca. 7.5 nm before final melting at 280 °C. Such two-step thickening in $l_c$ as marked by $T_{m1,\alpha}$ (245 °C) and $T_{m2,\alpha}$ (275 °C) in Figure 5c, however, is not as clear-cut as that observed for β crystals in Figure 2a, presumably due to the polydispersity in crystal size as revealed by the broader SAXS shoulder in Figure 5b and the highly broadened DSC endotherm in Figure 5c.

Shown in Figure 6 are the observed changes of reciprocal crystalline lamellar thickness ($l_c^{-1}$) with temperature for the four α-dominated specimens. The GT melting line, determined from the linear envelope formed by the final data points of the four specimens, extrapolates to $T_m$* = 294 ± 4 °C, which agrees well with those obtained by Ho et al.[5] (298 °C) or Wang et al.[7] (294 °C) using Marand's nonlinear extrapolation scheme. On the basis of the crystallinity-corrected $\Delta H_f$ = 79.3 ± 3.6 J/g = 81.9 ± 3.7 MJ m$^{-3}$ from parallel DSC/WAXS results (Figure 7), the fold surface energy of α crystals is determined from the slope of the melting line as $\sigma_{e,\alpha}$ = 8.2 ± 1.8 mJ m$^{-2}$. Reflecting the weaker thickness dependence of the melting temperature of α lamellae at temperatures below $T_{m2}$, this low value of fold surface energy of the α phase as compared to the case of β crystals (i.e., ca. 1/3 of $\sigma_{e,\beta}$) bears intricate implications to the fold surface structure (to be discussed later).

We have stated previously that the purity of all the α-dominated specimens used is better than 87% with some residual β phase.[4,38] Since the β phase melt slightly earlier (1 or 2 °C) than the α phase samples (results of this study and ref 17), the $l_c$ values measured at the *final* melting temperatures of the four α phase samples between 279 and 281 °C (Figure 5d) correspond solely to α crystals, so is the extrapolated $T_m$* value. As for crystallinity-related thermodynamic parameters of the pure α phase (Table 2), these are deduced from α-dominated specimens with corrections for the residual (≤13%) β crystals; i.e., we have subtracted the heat contributed by residual β crystals from the area under the endotherm of each α-dominated specimen to obtain the $\Delta H_f$ value of the pure α phase.

**Fold Energy.** We note first that the much lower $\sigma_{e,\alpha}$ value bears practical significance: it renders the formation of α nuclei *kinetically* competitive at a large supercooling where the *critical* lateral size $r_c$ for subsequent growth predominantly scales with $\sigma_e$. In comparison, the much higher $\sigma_{e,\beta}$ value renders the β phase more responsive to externally added heterogeneous nucleation agents such as nanoclays[39−42] or carbon nanocapsules.[43]

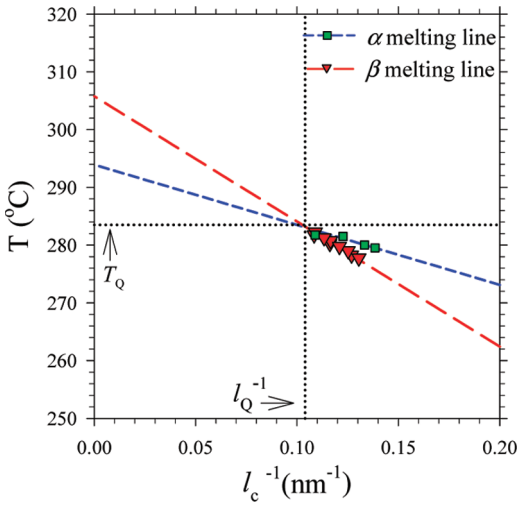


**Figure 8.** Circumstantial phase stability diagram constructed based on the two GT melting lines of the α and $\beta$ phases, which are determined from the final crystal thicknesses of the four α- and eight $\beta$-specimens, respectively. The two lines intersect at $T_Q = 284 \pm 2$ °C (horizontal dotted line) and $l_Q^{-1} = 0.104$ nm$^{-1}$ (vertical dotted line).

To facilitate comparison at the molecular level, we extract the fold energy $g = \sigma_e A/n_f$ for the α and $\beta$ phases from the corresponding values of $\sigma_e$ (8.2 vs 26.8 mJ m$^{-2}$), the unit cell base area $A$ (5.97 vs 2.53 nm$^2$), and the number of fold $n_f$ (4.5 vs 2), which result in $g_\alpha = 6.6 \pm 1.4$ kJ mol$^{-1}$ and $g_\beta = 20.4 \pm 1.4$ kJ mol$^{-1}$, the latter being comparable to that (ca. 19 kJ mol$^{-1}$) obtained by Chen et al.[20] from growth rate measurements (without specifying the phase, but likely the $\beta$ form in view of their experimental $T_{mc}$ range of 236−244 °C). Both $g$ values are much lower than the broad and similar range of estimates (45−90 kJ mol$^{-1}$) for the two phases by Napolitano and Pirozzi[44,45] via extensive molecular mechanics calculations based on various schemes of adjacently re-entered tight folds with different force fields. Nevertheless, the low $g$ values observed are consistent with the TEM observations[23] that decorating polyethylene crystals are randomly oriented on both α and $\beta$ basal planes, indicating that the folds are generally disordered. It is also consistent with the limited crystallinity (ca. 27%) development even after long-term isothermal crystallization. The disordered folds can be either nonadjacently re-entered (hence more switchboard-like) or loosely looped (hence more fringed micelle-like). We would expect α crystals to be closer to the fringed micelle end in view of the significantly lower density (by 3%) and hence milder congestion in the basal plane. In comparison, chain re-entry in $\beta$ crystals would expectedly correspond better to the random switchboard model, considering the extensive presence of packing disorder[2] and stacking faults.[46]

**Relative Phase Stability.** All the values of the thermodynamic parameters obtained for the α and $\beta$ phases are summarized in Table 2. Shown in Figure 8 is the relative phase stability diagram constructed based on the two melting lines of the two phases. The two lines intersect at $T_Q = 284 \pm 2$ °C, with the corresponding crystal thickness $l_Q = 9.6$ nm. The temperature $T_Q$ can be regarded as a stability inversion point where the relative thermal stability of the two phases reverses. For crystals with thicknesses $l_c > l_Q$, the $\beta$ form is the stable phase; for crystals with thicknesses $l_c < l_Q$, the α form is more stable. Consistent with this diagram, extensive results of our transmission electron microscopic (TEM) observations (over Pt-shadowed *thin-film* specimens isothermally treated at various temperatures) have indicated that thick crystals ($l_c = 11-14$ nm) are exclusively of the $\beta$ form whereas α crystals are usually thin (typically $l_c = 5-7$ nm). In the bulk specimens studied here, however, measured thicknesses of the $\beta$ crystals are comparable to those of α crystals, implying stronger effects from chain entanglement for $\beta$ crystals in the case of bulk crystallization.

**Comments on α-to-$\beta$ Transformation.** We start by re-emphasizing that the alleged α-to-$\beta$ transformation should not be a solid−solid transformation in view of the substantial density difference between the two phases. The volumetric strain induced by such transformation would eventually inhibit the process.[47] Should such a transformation occur at all, at least *some* partial melting must be involved, as suggested by Ho et al.[23]

According to the circumstantial phase stability diagram of sPS in Figure 8, it is indeed correct (as assumed by Ho et al.[5,23]) that $\beta$ crystals are more stable than α lamellae in the thick crystal limit (quantitatively specified here as $l_c > l_Q \approx 9.6$ nm). However, we have demonstrated that it is rather difficult for both polymorphs to reach this critical crystal thickness via bulk crystallization processes, in agreement with previous TEM results of microtomed specimens of bulk-crystallized samples.[8,25] The absence of α-to-$\beta$ phase transformation in the previous XRD studies of α-dominated thick specimens in the temperature range of 240−270 °C by de Rosa et al.[24] and 250−286 °C by Su et al.[17] may then be conveniently attributed to the presumably limited crystal thickness in bulk-crystallized specimens, which renders α crystals circumstantially more stable. The case of phase transformation observed with thin-film TEM specimens in the follow-up study of Ho et al.[23] cannot be directly related to the present work of bulk specimens. Nevertheless, our own TEM observations have indeed indicated frequent presence of $\beta$ crystals thicker than 10 nm in thin films, but it is hard to identify whether any of the $\beta$ crystals are transformed from the α form.

As a final point, we should emphasize that the values of thermodynamic parameters reported here and the discussion above are all based on the GT lines obtained near solid−liquid equilibration around 280 °C. These results should more properly be related to the ordered α″ and disordered $\beta'$ subforms according to our earlier high-temperature WAXS study.[17]

## Conclusion

Using simultaneous SAXS/WAXS/DSC, we have observed in situ the evolution of crystal thickness for α and $\beta$ crystals of sPS upon slow heating. The Kratky−Porod approximation has been successfully applied for determining the crystal thickness, especially when the stacked lamellae structure largely deteriorates into isolated lamellae as final melting is approached. The stability inversion at the crossover point ($T_Q$, $l_Q^{-1}$) = (284 °C, 0.104 nm$^{-1}$) of the two melting lines unambiguously defines the circumstantial metastability of the two phases. The high nucleation rate of fringed micelle-like α crystals at low temperatures (high supercoolings) and their reluctance to thickening are originated from the low basal surface energy. In contrast, the $\beta$ phase is hard to eliminate during bulk crystallization due to its higher $T_{m,\beta}$* and $\Delta H_{f,\beta}$, hence stronger driving force toward crystallization, whereas the higher basal surface energy $\sigma_{e,\beta}$ renders $\beta$ crystals more sensitive to externally added heterogeneous nucleation agents. While *thermodynamic* parameters quantitatively determined in this work provide a strong basis for general discussions of the phase behavior and the specific assignment of relative phase stability in bulk-crystallized sPS, issues in *kinetic* details of nucleation, growth, or lamellar thickening remain to be addressed in the future.

**Acknowledgment.** Financial support from the National Science Council (Grants NSC95-2221-E-007-267 and NSC96-2112-M-213-008-MY3) is gratefully acknowledged.

## References and Notes

(1) Ishihara, N.; Seimiya, T.; Kuramoto, M.; Uoi, M. *Macromolecules* **1986**, *19*, 2465.
(2) Woo, E. M.; Sun, Y. S.; Yang, C. P. *Prog. Polym. Sci.* **2001**, *26*, 945.
(3) Cartier, L.; Okihara, T.; Lotz, B. *Macromolecules* **1998**, *31*, 3303.
(4) Guerra, G.; Vitagliano, V. M.; De Rosa, C.; Petraccone, V.; Corradini, P. *Macromolecules* **1990**, *23*, 1539.
(5) Ho, R. M.; Lin, C. P.; Hseih, P. Y.; Chung, T. M.; Tsai, H. Y. *Macromolecules* **2000**, *33*, 6517.
(6) Lin, R. H.; Woo, E. M. *Polymer* **2000**, *41*, 121.
(7) Wang, C.; Hsu, Y. C.; Lo, C. F. *Polymer* **2001**, *42*, 8447.
(8) Wang, C.; Chen, C. C.; Hung, C. H.; Lin, K. S. *Polymer* **2004**, *45*, 6681.
(9) Arnauts, J.; Berghmans, H. *Polym. Commun.* **1990**, *31*, 343.
(10) Cimmino, S.; Di Pace, E.; Martuscelli, E.; Silvestre, C. *Polymer* **1991**, *32*, 1080.
(11) Yang, H.; Hsiao, B. *Polym. Mater. Sci. Eng.* **1999**, *81*, 285.
(12) Hoffman, J. D.; Weeks, J. J. *J. Res. Natl. Bur. Stand.* **1962**, *A66*, 13.
(13) Marand, H.; Xu, J.; Srinivas, S. *Macromolecules* **1998**, *31*, 8219.
(14) Xu, J.; Srinivas, S.; Marand, H. *Macromolecules* **1998**, *31*, 8230.
(15) Al-Hussein, M.; Strobl, G. *Macromolecules* **2002**, *35*, 1672.
(16) Alamo, R. G.; Viers, B. D.; Mandelkern, L. *Macromolecules* **1995**, *28*, 3205.
(17) Su, C. H.; Chen, S. H.; Su, A. C.; Tsai, J. C. *J. Polym. Res.* **2004**, *11*, 293.
(18) Gianotti, G.; Valvassori, A. *Polymer* **1990**, *31*, 473.
(19) Pastor, A. J.; Landes, B. G.; Karjala, B. G. *Thermochim. Acta* **1991**, *177*, 187.
(20) Chen, Q.; Yu, Y.; Na, T.; Zhang, H.; Mo, Z. *J. Appl. Polym. Sci.* **2002**, *83*, 2528.
(21) Van Hooy-Corstjens, C. S. J.; Hohne, G. W. H.; Rastogi, S. *Macromolecules* **2005**, *38*, 1814.
(22) Keller, A.; Cheng, S. Z. D. *Polymer* **1998**, *39*, 4461.
(23) Ho, R. M.; Lin, C. P.; Hseih, P. Y.; Chung, T. M.; Tsai, H. Y. *Macromolecules* **2001**, *34*, 6736.
(24) De Rosa, C.; de Ballesteros, O. R.; Di Dennaro, M.; Auriemma, F. *Polymer* **2003**, *44*, 1861.
(25) Wang, C.; Cheng, Y. W.; Hsu, Y. C.; Lin, T. L. *J. Polym. Sci., Polym. Phys.* **2002**, *40*, 1626.
(26) Strobl, G. *Prog. Polym. Sci.* **2006**, *31*, 938.
(27) Roe, R. J. *Methods of X-ray and Neutron Scattering in Polymer Science*; Oxford University Press: Oxford, 2000.
(28) Strobl, G. *The Physics of Polymers*; Springer: Berlin, 1996.
(29) Chen, Y. P.; Tsai, J. C.; Hong, J. L. *J. Chin. Chem. Soc.* **2003**, *50*, 205.
(30) Chuang, W. T.; Jeng, U.; Hong, P. D.; Lai, Y. H.; Shih, K. S. *Polymer* **2007**, *48*, 2919.
(31) Lai, Y. H.; Sun, Y. S.; Jeng, U.; Lin, J. M.; Lin, T. L.; Sheu, H. S.; Chuang, W. T.; Huang, Y. S.; Hsu, C. H.; Lee, M. T.; Lee, H. Y.; Liang, K. S.; Gabriel, A.; Koch, M. H. J. *J. Appl. Crystallogr.* **2006**, *39*, 871.
(32) Su, C. H.; Jeng, U.; Chen, S. H.; Lin, S. J.; Ou, Y. T.; Chuang, W. T.; Su, A. C. *Macromolecules* **2008**, *41*, 7630.
(33) Chuang, W. T.; Jeng, U.; Sheu, H. S.; Hong, P. D. *Macromol. Res.* **2006**, *14*, 45.
(34) Chen, S. H.; Lin, T. L. In *Methods of Experimental Physics - Neutron Scattering in Condensed Matter Research*; Skold, K., Price, D. L., Eds.; Academic: New York, 1987; Vol. 23B, Chapter 16.
(35) Glatter, O.; Kratky O. *Small Angel X-ray Scattering*; Academic Press: New York, 1980.
(36) Bassett, D. C.; Vaughan, A. S. *Polymer* **1986**, *27*, 1472.
(37) Basaet, D. C.; Olley, R. H.; AI Raheil, I. A. M. *Polymer* **1988**, *29*, 1745.
(38) Murphy, N. S.; Curran, S. A.; Aharoni, S. M.; Minor, H. *Macromolecules* **1991**, *24*, 3215.
(39) Tseng, C. R.; Lee, H. Y.; Chang, F. C. *J. Polym. Sci., Polym. Phys.* **2001**, *39*, 2097.
(40) Tseng, C. R.; Wu, J. Y.; Lee, H. Y.; Chang, F. C. *Polymer* **2001**, *42*, 10063.
(41) Wu, T. M.; Hsu, S. F.; Wu, J. Y. *J. Polym. Sci., Polym. Phys.* **2002**, *40*, 736.
(42) Wu, T. M.; Hsu, S. F.; Wu, J. Y. *J. Polym. Sci., Polym. Phys.* **2003**, *41*, 560.
(43) Wang, C.; Huang, C. L.; Chen, Y. C.; Hwang, G. L.; Tsai, S. J. *Polymer* **2008**, *49*, 5564.
(44) Napolitano, R.; Pirozzi, B. *Macromol. Theory Simul.* **2002**, *11*, 472.
(45) Napolitano, R.; Pirozzi, B. *Macromolecules* **2003**, *36*, 1368.
(46) Tosaka, M.; Hamada, N.; Tsuji, M.; Kohjiya, S.; Ogawa, T.; Isoda, S.; Kobayashi, T. *Macromolecules* **1997**, *30*, 4132.
(47) Chen, S. H.; Su, A. C.; Su, C. H.; Chen, S. A. *J. Phys. Chem. B* **2006**, *110*, 4007.